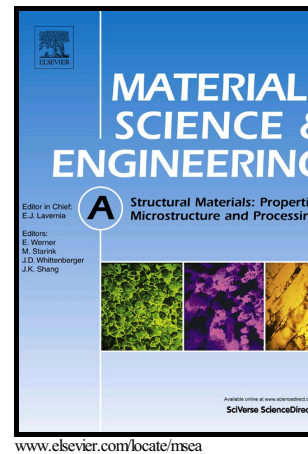


Author's Accepted Manuscript

Effect of grain size and specimen dimensions on micro-forming of High purity aluminum

Jie Xu, Xiaocheng Zhu, Debin Shan, Bin Guo, Terence G Langdon



PII: S0921-5093(15)30305-1
DOI: <http://dx.doi.org/10.1016/j.msea.2015.08.060>
Reference: MSA32694

To appear in: *Materials Science & Engineering A*

Received date: 25 June 2015
Revised date: 15 August 2015
Accepted date: 18 August 2015

Cite this article as: Jie Xu, Xiaocheng Zhu, Debin Shan, Bin Guo and Terence C Langdon, Effect of grain size and specimen dimensions on micro-forming of High purity aluminum, *Materials Science & Engineering A* <http://dx.doi.org/10.1016/j.msea.2015.08.060>

This is a PDF file of an unedited manuscript that has been accepted for publication. As a service to our customers we are providing this early version of the manuscript. The manuscript will undergo copyediting, typesetting, and review of the resulting galley proof before it is published in its final citable form. Please note that during the production process errors may be discovered which could affect the content, and all legal disclaimers that apply to the journal pertain

Submitted to Mater Sci Eng A (June 2015): revised July 2015; second revision August 2015

Effect of grain size and specimen dimensions on micro-forming of high purity aluminum

Jie Xu^{1,2,3}, Xiaocheng Zhu^{1,2}, Debin Shan^{1,2}, Bin Guo^{1,2*}, Terence G Langdon^{3,4*}

1. Key Laboratory of Micro-systems and Micro-structures Manufacturing of Ministry of Education, Harbin Institute of Technology, Harbin, 150080, China;
2. School of Materials Science and Engineering, Harbin Institute of Technology, Harbin, 150080, China
3. Departments of Aerospace & Mechanical Engineering and Materials Science, University of Southern California, Los Angeles, CA 90089-1453, USA
4. Materials Research Group, Faculty of Engineering and the Environment, University of Southampton, Southampton SO17 1BJ, UK

Abstract

Micro-compression testing was conducted using high purity Al processed by equal-channel angular pressing (ECAP) with both coarse-grained (CG) and ultrafine-grained (UFG) samples. The effects on the flow stresses of the initial grain size and the specimen size were investigated and the results show the initial grain sizes and the specimen dimensions affect the flow stresses during micro-compression for both CG and UFG specimens. There is a transition from strain hardening to strain softening with decreasing grain size during micro-compression but the transition grain size is dependent upon the size of the specimen. These results are interpreted using a model based on the separate influences of dislocation annihilation and dislocation accumulation in the UFG and CG materials, respectively. The results demonstrate that the occurrence of surface roughening is improved when using UFG pure Al and this shows there is a significant potential for using UFG pure Al in micro-forming operations.

Keywords: aluminum; equal-channel angular pressing; micro-forming; size effects; ultrafine grains

*Corresponding authors at: E-mail: bguo@hit.edu.cn (B. Guo); langdon@usc.edu (T. G. Langdon)

1. Introduction

Over the last twenty years, the fundamental requirements for the fabrication of micro-parts have increased significantly due primarily to the rapid development of micro-electro-mechanical systems (MEMS). Micro-manufacturing is now becoming an important technology due to the increasing trend for miniaturization where micro-forming is defined as the production of parts or structures having at least two dimensions in the sub-millimeter range. In practice, micro-forming is rapidly becoming one of the promising micro-manufacturing techniques due to the potentials for high productivity, low cost and good mechanical properties [1-3].

Nevertheless, although the knowledge of tool design and fabrication methods are now well established for conventional macro-forming, there is evidence that the presence of size effects may lead to a breakdown in these basic manufacturing characteristics when the specimen dimensions are scaled down to the micro-scale [4, 5]. To date, significant attention has been directed to examining the geometry size effects in micro-deformation [6]. For example, it was shown that the flow stress increases with decreasing specimen thickness when the ratio of specimen size to grain size is reduced below a critical value [7]. Similar results were also reported for several different materials [8-10]. In an investigation of the influence on mechanical properties and strain hardening of the material thickness and grain size, and specifically on the thickness to grain size ratio, it was shown that three deformation domains may be identified [11]: these domains were specifically designated as polycrystalline, multicrystalline and quasi-single crystalline, where the designations depend upon the thickness and the numbers of grains across the sample thickness. A study of size effects in miniaturized polycrystalline samples indicated that grain size, grain orientation and the nature of the

grain boundaries all play important roles in delineating the intrinsic competition between the strengthening and weakening contributions [12].

As a consequence of the ongoing and increasing need for miniaturization, the grain size of conventional coarse-grained (CG) materials, which is typically a few to several tens of microns, becomes reduced to the same scale and with the characteristic dimensions of the micro-parts. In practice, if only a few grains are present in the micro-component then the response to the applied forces will show significant variations such that the reproducibility of the mechanical properties will become a serious problem in any micro-forming operation [13]. It follows, therefore, that these size effects are critical and must be considered in micro-forming in order to fabricate high quality micro-components.

By comparison with CG materials, ultrafine-grained (UFG) materials have the potential for simultaneously fulfilling two important conditions [14]. First, the average grain size is generally smaller than the smallest dimension of the component and this guarantees reproducible properties. Second, the grain size is sufficiently fine to ensure a high strength and fracture toughness. In addition, it is anticipated that materials with ultrafine grains will exhibit good formability over appropriate ranges of temperature and strain rate [15]. Therefore, it is reasonable to conclude that the grain size is the dominant factor determining the limiting size of the geometrical features that may be conveniently fabricated by micro-forming and this means in practice that very small grain sizes, and especially materials having ultrafine submicrometer grain sizes, are attractive for use in micro-forming operations.

It is now well established that UFG materials are most easily produced through the application of severe plastic deformation (SPD) to large bulk samples [16] using processes such as equal-channel angular pressing (ECAP) [17] and high-pressure torsion (HPT) [18]. Recent research has

demonstrated the potential for using UFG materials for applications in micro-forming at elevated and ambient temperatures [19, 20]. Nevertheless, only very limited information is at present available on the micro-forming deformation behavior when the material grain size is reduced to the sub-micrometer level although these problems are beginning to attract attention within the materials science community [21-24].

The present research was initiated specifically to examine the micro-compression behavior of high purity aluminum having grain sizes from the ultrafine scale to the coarse scale achieved by ECAP processing and annealing treatments. The surface roughness and microstructural evolution after micro-compression were investigated for both UFG and CG pure Al and the effects on the deformation mechanism of the initial grain size and specimen dimensions were critically analyzed.

2. Experimental material and procedures

Pure aluminum of very high purity (99.999%) was used in this investigation. The high purity aluminum was supplied in the form of drawn rods having diameters of 10 mm and lengths of ~70 mm. These rods were annealed in air for 1 hour at a temperature of 773 K to obtain an initial grain size of ~300 μm . The experimental investigation followed four separate steps as illustrated schematically in Fig. 1.

In the first step, processing by ECAP was conducted at room temperature using a die with an internal angle of 90° between the two parts of the channel and an outer arc of curvature of 20° at the point of intersection [25]. This geometry leads to an imposed strain of ~1.0 on each separate pass through the die [26]. The billets were sprayed with an MoS_2 lubricant and processed repetitively by ECAP through 8 passes corresponding to a maximum imposed strain of ~8. All samples were

processed using route B_C in which the sample is rotated by 90° in the same direction between each pass [27] where this processing route was selected because it leads most expeditiously to an array of equiaxed grains separated by a high fraction of high-angle grain boundaries [28].

In the second step following ECAP, billets were machined along the extrusion direction (ED) by electric discharge machining (EDM) to give small cylinders having dimensions of 4 (diameter) × 6 (height), 2 × 3 and 1 × 1.5 mm × mm. The transverse direction (TD) was located randomly for this machining and this is reasonable based on the lack of any orientation dependence of hardness measurements after processing by ECAP [29]. The specimens were then prepared by micro-forward extrusion at room temperature using three different dimensional tools with diameters of 2, 1 and 0.5 mm. These extruded billets were cut and ground to form micro-compression specimens having good dimensional accuracy with specimen diameter, D , × specimen height, H_0 , of 2 × 3, 1 × 1.5 and 0.5 × 0.75 mm × mm, respectively.

Before micro-compression testing, the micro-compression specimens were annealed for 1 hour at temperatures of 423, 573, 673 or 773 K, respectively, and the microstructures were then observed using an FEI Quanta 200FEG field emission scanning electron microscope (FESEM) with the data analyzed using a TSL OIM system. Samples were prepared for the microstructural observations by slicing the as-pressed billets perpendicular to the pressing direction to give disks having thicknesses of ~3 mm. One side of each disk was ground on SiC papers and mechanically polished with 0.5 μm diamond paste and the disks were then electro-polished to mirror-like surfaces using a solution of 10% HClO₄ and 90% C₂H₅OH with a DC voltage of 35 V under a temperature of 253 K. This procedure is summarized as the third step in Fig. 1.

In order to remove the scratches formed by grinding, all samples were electro-polished to smooth surfaces using the same solution and conditions in the fourth step in Fig. 1. Ultimately, micro-compression testing was conducted with engineering strains, ϵ , of 30% or 50% using an Instron machine at room temperature (~ 298 K) with initial strain rates in the range from 3.3×10^{-4} to 0.1 s^{-1} . No lubricants were used during these tests in order to avoid any frictional effects on the flow stresses [30] and finally the surface morphologies were examined using FESEM.

3. Experimental results

3.1 Microstructural characteristics after processing

Representative OIM images are shown in Fig. 2 for micro-compression specimens after processing by ECAP through 8 passes and micro-extrusion (a) without additional annealing and after annealing for 1 hour at (b) 423, (c) 573, (d) 673 and (e) 773 K, respectively. The average grain sizes, d , were calculated directly from the OIM images using grain-to-grain instead of pixel-to-pixel measurements [31] and these values are recorded in the top row of Table 1. The grain size of $\sim 1.3 \mu\text{m}$ obtained from processing by ECAP through 8 passes is directly consistent with several reports describing the processing of pure Al by ECAP [32-36]. It should be noted from Fig. 2(a) that there is little or no change in grain size after the micro-compression so that the influence of the micro-extrusion may be neglected.

Following the annealing treatment, the grain size increased from $\sim 1.5 \mu\text{m}$ at 423 K to a maximum of $\sim 150 \mu\text{m}$ at 773 K. The Taylor factor was analyzed by OIM using a slip system of $\{111\}\langle 1-10\rangle$ and a deformation gradient for uniaxial compression. The average Taylor factor, M , after processing by ECAP was about 3.06 which is equal to the value for untextured polycrystalline face-centered cubic

(f.c.c.) metals. With increasing annealing temperature, the average values of M decreased to 2.64 at 673 K and then abnormally increased to 3.19 at 773 K. These values are given in the bottom row of Table 1 and the two middle rows summarize the measured percentage fractions of low-angle grain boundaries (LAGBs) and high-angle grain boundaries (HAGBs).

3.2 *The stress-strain behavior*

The relationship between true stress and true strain is shown in Fig. 3 for the micro-compression samples with a diameter of 2 mm for different grain sizes of (a) 1.5 and (b) 150 μm at strain rates from 3.3×10^{-4} to 0.1 s^{-1} . For all testing conditions, the true stress at a true strain of ~ 0.3 after micro-compression decreases with decreasing strain rate which corresponds to the deformation behavior after micro-tensile testing with CG materials [37]. An obvious yield phenomenon is evident in the curves for the UFG material shown in Fig. 3(a) but this is not apparent in the curves for the CG aluminum shown in Fig. 3(b). In addition, there is no clearly defined effect of strain rate on yield stress for the CG material and also for the UFG material except at the highest strain rate of 0.1 s^{-1} . However, it is readily apparent that the yield strength decreases from $\sim 120 \text{ MPa}$ for the UFG Al to $\sim 25 \text{ MPa}$ for CG Al and this confirms that the grain size is a dominant factor which determines the micro-deformation behavior.

Plots of true stress versus true strain are shown in Fig. 4 for different specimen diameters in micro-compression using samples with grain sizes of (a) 1.3, (b) 4.0 and (c) 150 μm . The results show that, as noted also in earlier experiments [38,39], the true stress decreases with decreasing specimen diameter not only for the conventional CG material but also for the UFG Al. These results demonstrate that the specimen dimension has a significant effect on the micro-compression behavior

which means that a size effect continues to exist even in the micro-deformation of UFG materials. In addition, the true stress increases with increasing true strain for the micro-compression samples with 2 mm diameter which demonstrates the occurrence of strain hardening. Nevertheless, there is clear evidence of strain weakening with decreasing specimen diameter and this weakening becomes more obvious with decreasing grain size for the specimens having the smallest diameter of 0.5 mm. These results confirm, therefore, that the deformation mechanism in UFG aluminum is different from that in conventional CG aluminum.

Figure 5 shows plots of true stress versus true strain of micro-compression testing with different grain sizes for specimen diameters of (a) 2, (b) 1 and (c) 0.5 mm at a strain rate of $1.0 \times 10^{-2} \text{ s}^{-1}$ using an engineering strain of 30%. The results show that the UFG Al without an annealing treatment exhibits the highest yield stress and flow stress and also that the flow stress and yield stress decrease with increasing grain size from 1.3 to 25 μm where the latter is consistent with results from cold-drawn specimens [39] and ECAP samples [40]. However, the flow stress and yield stress for a grain size of 150 μm are larger than after micro-compression testing of specimens with a grain size of 25 μm . The results are generally similar for all samples with different specimen sizes of 2, 1 and 0.5 mm. Furthermore, there is an obvious transition in Fig. 5 from strain hardening to strain weakening with decreasing grain size.

3.3 The surface topography recorded by SEM

Figure 6 shows the surface topographies of the compressed specimens with diameters of 2, 1 and 0.5 mm and grain sizes from ~ 1.3 to $\sim 150 \mu\text{m}$. Inspection shows that the geometries of the compressed samples become irregular with micro-compression testing. Thus, the surfaces are not

circular for the CG Al with a grain size of 150 μm and a diameter of 2 mm as shown in Fig. 6(a) and the geometries become more irregular with decreasing specimen size as shown in Fig. 6(b)-(c). Inspection of Fig. 6(c) shows the occurrence of folding in the compressed micro-size specimen with a diameter of 0.5 mm.

By comparison with the CG Al, the non-uniform deformation may be improved significantly by decreasing the grain size from 25 to 1.3 μm as shown in Fig. 6(d)-(g) where the compressed specimens are cylindrical with smooth surfaces. The non-uniform deformation improves with decreasing grain size for both the macro-size and the micro-size specimens as shown in Fig. 6(d)-(i) and the decrease in non-uniformity of the compressed specimens of macro-size is more significant than for compressed specimens of micro-size. Finally, it is apparent from Fig. 6 that the surface roughening increases with increasing grain size for both the macro-size and micro-size specimens and the surface roughness increases with decreasing specimen size.

3.4 Microstructural observations by EBSD

Detailed microstructural information is given in Fig. 7 for pure Al with a grain size of 1.5 μm and the same information is given in Fig. 8 for the material with a grain size of 25 μm . In both displays, the microstructures are shown in (a-c) along the compressive direction near the centers of the compressed samples and the misorientation angle distributions in (d-f) were recorded at the centers of the samples using grain-to-grain measurements which lead to abnormally high fractions recorded in each distribution at the lowest recorded angle [31].

In Fig. 7(a), (b) and (c) the microstructures are shown after 50% micro-compression with initial specimen diameters of (a) 2, (b) 1 and (c) 0.5 mm and Fig. 7(d), (e) and (f) provide the corresponding

misorientation angle distributions. It should be noted that these specimens were deformed to 50% specifically for surface topography by SEM but in practice there was no clear difference between the 30% and 50% samples.

It is readily apparent that ultrafine grains with average sizes of $\sim 1.0 \mu\text{m}$ remain at the center after micro-compression although the grains are slightly elongated in the radial direction. The average value of the misorientation angles remains essentially constant at $\sim 27\%$ for each specimen size and the misorientation angle distributions remain unchanged for the fractions of LAGBs ($2-15^\circ$) and HAGBs ($>15^\circ$) which is similar to the misorientation angle distribution of the initial specimen before micro-compression testing. The high fraction of HAGBs suggests that grain boundary sliding (GBS) and grain rotation may be important deformation mechanisms during the micro-compression of UFG pure aluminum. It should be noted that this conclusion is consistent with other experimental data on UFG pure Al showing the occurrence of GBS at room temperature during micro-compression of cold-rolled pure copper [38], depth-sensing indentation of UFG pure Al [40,41] and tensile testing of UFG pure Al [42,43] and with data showing GBS in a UFG Al-30% Zn alloy processed by HPT and then compressed as micro-pillars [44,45].

Similar results are shown in Fig. 8 after annealing at 673 K to produce a grain size of $25 \mu\text{m}$. Figure 8(a) shows the microstructure at the center of the sample after 50% micro-compression with an initial diameter of 2 mm where some of the initial grain boundaries are marked by white arrows and the surrounding grains are generally elongated perpendicular to the compressive direction. Within the elongated initial grains, many sub-grains of almost equal size are newly generated and delineated by LAGBs that are indicated by yellow lines. In addition, some new small grains with HAGBs are

formed near the initial grain boundaries. In Fig. 8(b) for a diameter of 1 mm, there are many fine grains and sub-grain boundaries but the original larger grains remain in the upper area of the compressed sample which compares with the uncompressed sample shown in Fig. 2(d). For a specimen size of 0.5 mm in diameter, Fig. 8(c) shows the microstructural features similar to the results in Fig. 8(b) with a 1 mm diameter. For the misorientation angle distributions, the average value of the misorientation angles increases from ~13% to ~16% with decreasing specimen diameters from 2 to 0.5 mm after 50% micro-compression. The fractions of LAGBs decrease from ~72% to ~66% and the fraction of HAGBs increases from ~28% to ~34% with decreasing specimen size from 2 to 0.5 mm which is different from the misorientation angle distribution of the initial specimen before micro-compression testing.

4. Discussion

4.1 Strengthening behavior during micro-compression of pure Al

It is readily apparent from Fig. 5 that there are two different strengthening behaviors in UFG pure Al. The first strengthening mechanism is grain size dependent and arises because the grain boundaries represent obstacles to easy slip transfer [47]. This effect derives from the Hall-Petch relationship which is given by [48,49]

$$\sigma_y = \sigma_0 + k_1 d^{-1/2} \quad (1)$$

where σ_y is the yield or flow stress, d is the grain size and σ_0 and k_1 are constants.

To check on the applicability of this relationship, the values of the true stress are plotted against $d^{1/2}$ in Fig. 9 for specimen diameters of (a) 2, (b) 1 and (c) 0.5 mm. All of these plots are mutually consistent and they demonstrate that the Hall-Petch relationship is valid for all specimen sizes when

$d^{1/2} > 0.2 \mu\text{m}^{-1/2}$ but there is a marked increase in the Hall-Petch slope at the largest grain size.

The deviation in the Hall-Petch plot in Fig. 9 for a grain size of $\sim 150 \mu\text{m}$ at $d^{1/2} = 0.08 \mu\text{m}^{-1/2}$ appears to be affected by specimen size such that the deviation is reduced with decreasing size from 2 to 0.5 mm. At large strain, many of the LAGBs evolve into HAGBs which are then indistinguishable from the original grain boundaries so that, assuming an identical strengthening for these two types of boundaries, the value of d is replaced by d_{HAGB} and the new flow stress, σ_f , may be expressed as [50]

$$\sigma_f = \sigma_0 + M\alpha G \sqrt{1.5b(S_V\theta)_{\text{LAGB}}} + k_1(\varepsilon)d_{\text{HAGB}}^{-1/2} \quad (2)$$

where σ_0 is the appropriate friction stress, α is a constant, G is the shear modulus, b is the Burgers vector, S_V is the area of boundaries per unit volume and θ is the misorientation angle. Thus, the flow stress is related to the contributions from both LAGBs and HAGBs [51]. When the grain size is less than $4 \mu\text{m}$, the contribution of LAGBs may be neglected due to the small fraction of LAGBs and the flow stress is then effectively described by eq. (1). However, when the grain size is of the order of $\sim 25 \mu\text{m}$, the fraction of LAGBs is larger than the fraction of HAGBs and the distribution of LAGBs cannot be neglected. In addition, the contribution of LAGBs becomes larger due to the higher fraction of LAGBs of 68% when the grain size is further increased to $150 \mu\text{m}$.

As documented in Table 1, the Taylor factor M of pure Al with a grain size of $\sim 150 \mu\text{m}$ is ~ 3.2 which is larger than the Taylor factor of ~ 2.6 for pure Al with a grain size of $\sim 25 \mu\text{m}$. It is well established that large values of M indicate that deformation requires large amounts of slip and expends plastic work through the deformation of grains in hard orientations [52]. In practice, the stress required to deform these hard orientation grains is much larger than for soft orientation grains in f.c.c. metals [53]. Thus, it follows from eq. (2) that the flow stress after micro-compression for pure Al

with coarser grains of $\sim 150 \mu\text{m}$ is larger than for a grain size of $\sim 25 \mu\text{m}$ as demonstrated in Fig. 5.

4.2 Softening behavior in the micro-compression of pure Al

There is a softening behavior in the flow stress with a reduction in the specimen size in Fig. 4 both for the specimen of CG pure Al with a grain size of $\sim 150 \mu\text{m}$ and for specimens of UFG pure Al with a grain size of $\sim 1.5 \mu\text{m}$. Reductions in the flow stress in micro-compression and micro-tensile testing was investigated extensively in earlier experiments [54-57] and it appears that the specimen size effect is only significant when the sample size decreases to dimensions comparable to about 10 times the average grain size [3]. Nevertheless, the present investigation provides clear evidence for softening behavior in the UFG pure Al. It is now established that a mechanical behavior modification with a strong decrease in flow stress may arise from a soft surface layer effect for specimens having less than four grains across the thickness [11].

Accordingly, a surface layer model can be presented to explain the specimen size effect on flow stress as depicted in Fig. 10 which is based on a combination of grain boundary strengthening and surface grain effects [37,58-60]. The model assumes that the deformation behavior of the surface grains is different from the internal grains since the surface grains are less constrained [7,61]. It follows from this model that the decrease in flow stress with decreasing specimen size is then attributed to the increase in the volume fraction of the surface layer with decreasing D . Using this surface layer model, the flow stress may be described by considering the relative contributions of the surface grains, the constrained grains and the internal grains through the expression

$$\sigma(\varepsilon) = f_s \sigma_s(\varepsilon) + f_c \sigma_c(\varepsilon) + f_i \sigma_i(\varepsilon) \quad (3)$$

where $\sigma_s(\varepsilon)$, $\sigma_c(\varepsilon)$, and $\sigma_i(\varepsilon)$ are the flow stresses of the surface grains, constrained grains and

internal grains, respectively, and f_s , f_c , and f_i are the corresponding volume fractions of the surface grains, constrained grains and internal grains, respectively. The volume fraction of surface grains increases with decreasing specimen size and it is known that the flow stress of the surface grains is lower than for the internal grains and constrained grains [38] since grain boundary sliding becomes dominant for the less constrained surface grains. This approach also follows, and is consistent with, the conventional interpretation of grain boundary sliding in polycrystalline materials where it is well established that there are differences in the sliding behavior between surface grains and internal grains [62]. It follows therefore that the flow stress in micro-compression is anticipated to decrease with decreasing specimen size. In addition, the flow stresses at a true strain of ~ 0.3 are reduced to ~ 46 and ~ 45 MPa for CG pure Al with average grain sizes of ~ 150 and ~ 4 μm , respectively, and there is a corresponding reduction to ~ 56 MPa in UFG pure Al with a grain size of ~ 1.3 μm when the specimen size is reduced from 2 to 0.5 mm as shown in Fig. 4. These results show that the UFG pure Al has a much higher reduction in flow stress during the micro-compression testing.

It should be noted that there is also another type of softening which is different from the specimen size effect. Figure 4 shows there is a transition from strain hardening to strain softening during micro-compression with decreasing grain size and this is especially evident when testing UFG pure Al at the micro-scale specimen size with a diameter of 0.5 mm. It is apparent from Fig. 6(a) that the flow stress decreases with increasing true strain during micro-compression of pure Al with an average grain size of $\sim 1.3\mu\text{m}$ and Fig. 11 shows representative TEM microstructures at the center of compressed samples of UFG pure Al and CG pure Al. Thus, the grain shape is different between these two samples where the grains are elongated in the compressive deformation in the CG pure Al but the

grains remain ultrafine and essentially equiaxed in the UFG pure Al. These features agree with those microstructures observed by EBSD shown in Figs 7 and 8. For the CG pure Al samples, many dislocations are visible and there are sub-grain boundaries within the grains whereas for the UFG pure Al samples there are relatively few dislocations within the grains. It is considered that the dislocations introduced by compression are easily annihilated at grain boundaries since there are many HAGBs in the UFG pure Al and this leads to the consequent softening behavior during micro-compression.

Based on the results from this investigation, it is possible to develop a schematic illustration of the effect of the initial grain size on the stress-strain behavior in unidirectional compression as shown in Fig. 12. Initially, in the early stages of compression of the UFG aluminum, dislocations accumulate at the initial grain boundaries leading to an increase in the flow stress. With a further increase of the imposed strain, the dislocations are annihilated at the many HAGBs in the deformed material. This leads to a decrease in the flow stress and a consequent softening behavior during micro-compression. By contrast, dislocation accumulation leads to sub-grain boundary formation in the coarser grains of the CG pure Al and these sub-grain boundaries hinder the passage of dislocations leading to a consequent hardening. The schematic illustration in Fig. 12 provides an excellent match to the experimental results shown in Fig. 5.

4.3 The surface roughening effect in micro-compression of pure Al

The development of surface roughening during micro-compression is important because it affects adversely not only the overall ease of formability but also the reliability of the finished product since an increase in roughness may initiate strain localization leading to cracking in the micro-formed product.

In addition, the occurrence of surface roughening accelerates tool wear due to the increase in interfacial friction. Thus, the size effect on surface roughening becomes an important factor in practical applications and must be considered when undertaking all micro-forming operations.

Earlier studies noted that the local deformation may vary significantly both within the grains and among the arrays of grains so that restrictions near the grain boundaries can lead to grooving on the surfaces of compressed specimens [39]. The surface roughening phenomenon was very obvious in this investigation after micro-compression of CG pure Al for both the macro-size and the micro-size specimens and it is readily evident from inspection of the surface topographies of the compressed samples shown in Fig. 6. Furthermore, the geometries of the compressed samples become more irregular with decreasing specimen size, not only for CG pure Al but also for the UFG pure Al.

There are several reasons for the development of surface roughness in the micro-compression of pure Al. First, the deformation accommodated by slip bands generated during micro-compression may increase the surface roughness in CG pure Al as shown in Fig. 6 (a)-(c). Second, the surface grains are not sufficiently constrained so that grain boundary sliding occurs easily during the micro-compression and the resultant sharp offsets at the boundaries also increase the level of surface roughness. Third, the strain incompatibilities between adjacent grains may also cause inhomogeneities in the deformation, including folding when the free surface grains move normal to the surface. Therefore, it follows that the surface roughening behavior is related in a complex way to the specimen size, the grain size and the specific crystallographic orientations within the grains. Nevertheless, a surface roughening effect was not observed in the micro-compression of the UFG pure Al specimens as shown in Figs 6(d)-(i). This provides a clear demonstration that the ultrafine grains

improve the deformation compatibility.

The present results give direct demonstrations of the advantages and the potential applications associated with the micro-forming of UFG pure Al by comparison with using conventional CG pure Al. Furthermore, although the present UFG structures were obtained exclusively by using conventional processing by ECAP, it is reasonable to anticipate that the advantages of UFG microstructures will be equally apparent when processing samples using the ECAP-Conform process [63,64] or using HPT for the processing of bulk [65,66] or strip [67] samples.

5. Summary and conclusions

1. Experiments on aluminum of very high purity show that the initial grain sizes and the specimen dimensions affect the flow stresses during micro-compression of both CG and UFG specimens. The flow stress increases with decreasing grain size and with increasing specimen dimensions.

2. There is a transition from strain hardening to strain softening in the flow stress curves during micro-compression with decreasing of grain size, especially for the micro-compression testing of UFG pure Al at the micro-scale.

3. Dislocation annihilation leads to a decreasing flow stress and a softening behavior during micro-compression in UFG pure Al. By contrast, dislocation accumulation leads to the formation of sub-grain boundaries in CG pure Al and these boundaries hinder the dislocation movement increase the flow stress in the coarser-grained material.

4. Surface roughening is related to the specimen size, the grain size and the crystallographic orientations within the grains. The occurrence of roughening is improved when using UFG pure Al due to the improvement in strain compatibility between adjacent grains. These results demonstrate

the potential application for using UFG pure Al processed by ECAP in micro-forming operations.

Acknowledgements

This work was supported by the National Natural Science Foundation of China under Grant No. 51105102 and 51375111, the National Science Foundation of the United States under Grant No. DMR-1160966 and the European Research Council under ERC Grant Agreement No. 267464-SPDMETALS. Partial support was also provided by the National Basic Research Program of China under Grant No. 2012CB934100.

Accepted manuscript

References

- [1] M. Geiger, M. Kleiner, R. Eckstein, N. Tiesler, U. Engel, *CIRP Ann – Manuf. Techn.* 50 (2001) 445– 462.
- [2] U. Engel, R. Eckstein, *J. Mater. Process. Tech.* 35 (2002) 125– 126.
- [3] F. Vollertsen, H.S. Niehoff, Z. Hu, *Int. J. Mach. Tool. Manu.* 46 (2006) 1172– 1179.
- [4] F. Vollertsen, D. Biermann, H.N. Hansen, I.S. Jawahir, K. Kuzman, *CIRP Ann–Manuf. Techn.* 58 (2009) 566– 587.
- [5] M.W. Fu, W.L. Chan, *Int. J. Adv. Manuf. Tech.* 67 (2013) 2411– 2437.
- [6] E. Arzt, *Acta Mater.* 46 (1998) 5611– 5626.
- [7] S. Miyazaki, K. Shibata, H. Fujita, *Acta Metall.* 27 (1979) 855– 862.
- [8] L.V. Raulea, A.M. Goijaerts, L.E. Govaert, F.P.T. Baaijens, *J. Mater. Process. Tech.* 115 (2001) 44– 48.
- [9] T.A. Kals, R. Eckstein, *J. Mater. Process. Tech.* 103 (2000) 95– 101.
- [10] J.F. Michel, P. Picart, *J. Mater. Process. Tech.* 141 (2003) 439– 446.
- [11] C. Keller, E. Hug, X. Feaugas, *Int. J. Plast.* 27 (2011) 635– 654.
- [12] M.G.D. Geers, W.A.M. Brekelmans, P.J.M. Janssen, *Int. J. Solids. Struct.* 43 (2006) 7304– 7321.
- [13] P.J.M. Janssen, T.H. De Keijser, M.G.D. Geers, *Mater. Sci. Eng. A419* (2006) 238– 248.
- [14] Y. Estrin, M. Janecek, G.I. Raab, R.Z. Valiev, A. Zi. *Metall. Mater. Trans. A38* (2007) 1906– 1909.
- [15] M.S. Yeh, H.Y. Lin, H.T. Lin, C.B. Chang, *J. Mater. Process. Tech.* 180 (2006) 17– 22.
- [16] T.G. Langdon, *Acta Mater.* 61 (2013) 7035– 7059.
- [17] R.Z. Valiev, T.G. Langdon, *Prog. Mater. Sci.* 51 (2006) 881– 981.

- [18] A.P. Zhilyaev, T.G. Langdon, *Prog. Mater. Sci.* 53 (2008) 893– 979.
- [19] J. Xu, M. Shirooyeh, J. Wongsangam, D. Shan, B. Guo, T.G. Langdon, *Mater. Sci. Eng. A586* (2013) 108– 114.
- [20] J. Xu, X. Zhu, L. Shi, D. Shan, B. Guo, T.G. Langdon, *Adv. Eng. Mater.* (2015) DOI: 10.1002/adem.201400448
- [21] I. Sabirov, Y. Estrin, M.R. Barnett, T. Timokhina, P.D. Hodgson, *Acta Mater.* 56 (2008) 2223– 2230.
- [22] J.H. Schneibel, M. Heilmaier, W. Blum, G. Hasemann, T. Shanmugasundaram, *Acta Mater.* 59 (2011) 1300– 1308.
- [23] G.M. Le, A. Godfrey, N. Hansen, W. Liu, G. Winther, X. Huang, *Acta Mater.* 61 (2013) 7072– 7086.
- [24] N. Warthi, P. Ghosh, A.H. Chokshi, *Scripta Mater.* 68 (2013) 225– 228.
- [25] Y. Huang, T.G. Langdon, *Mater. Today* 16 (2013) 85-93.
- [26] Y. Iwahashi, J. Wang, Z. Horita, M. Nemoto, T.G. Langdon, *Scripta Mater.* 35 (1996) 143– 146.
- [27] M. Furukawa, Y. Iwahashi, Z. Horita, M. Nemoto, T.G. Langdon, *Mater. Sci. Eng. A257* (1998) 328– 332.
- [28] K. Ohishi, Z. Horita, M. Nemoto, T.G. Langdon, *Metall. Mater. Trans. A29* (1998) 2011– 2013.
- [29] J. Wongsangam, M. Kawasaki, T.G. Langdon, *Mater. Sci. Eng. A556* (2012) 526– 532.
- [30] B. Guo, F. Gong, C. Wang, D. Shan, *Trans. Nonferr. Metal. Soc.* 19 (2009) 516– 520.
- [31] L.S. Tóth, B. Beausir, C.F. Gu, Y. Estrin, N. Scheerbaum, C.H.J. Davies, *Acta Mater.* 58 (2010) 6706– 6716.

- [32] Y. Iwahashi, Z. Horita, M. Nemoto, T.G. Langdon, *Acta Mater.* 45 (1997) 4733– 4741.
- [33] Y. Iwahashi, Z. Horita, M. Nemoto, T.G. Langdon, *Acta Mater.* 46 (1998) 3317– 3331.
- [34] S.D. Terhune, D.L. Swisher, K. Oh-ishi, Z. Horita, T.G. Langdon, T.R. McNelley, *Metall. Mater. Trans.* 33A (2002) 2173– 2184.
- [35] A.A. Salem, T.G. Langdon, T.R. McNelley, S.R. Kalidindi, S.L. Semiatin, *Metall. Mater. Trans.* 37A (2006) 2879– 2891.
- [36] A.P. Zhilyaev, D.L. Swisher, K. Oh-ishi, T.G. Langdon, T.R. McNelley, *Mater. Sci. Eng. A429* (2006) 137– 148.
- [37] J. Xu, B. Guo, D. Shan, T.G. Langdon, *Mater. Sci. Forum* 783–786 (2014) 2726– 2731.
- [38] M. Geiger, F. Vollertsen, R. Kals, *CIRP Ann. – Manuf. Techn.* 45 (1996) 277– 282.
- [39] W.L. Chan, M.W. Fu, B. Yang, *Mater. Sci. Eng. A534* (2012) 374– 383.
- [40] T. Inoue, Z. Horita, H. Somekawa, K. Ogawa, *Acta Mater.* 56 (2008) 6291– 6303.
- [41] N.Q. Chinh, P. Szommer, T. Csanádi, T.G. Langdon, *Mater. Sci. Eng. A434* (2006) 326– 344 .
- [42] N.Q. Chinh, P. Szommer, Z. Horita, T.G. Langdon, *Adv. Mater.* 18 (2006) 34– 39.
- [43] K.V. Ivanov, E.V. Naydenkin, *Mater. Sci. Eng. A606* (2014) 313– 321.
- [44] K.V. Ivanov, E.V. Naydenkin, *IOP Conf. Series Mater. Sci. Eng.* 63 (2014) 012123.
- [45] N.Q. Chinh, T. Gyö ri, R.Z. Valiev, P. Szommer, G. Varga, K. Havancsák, T.G. Langdon, *MRS Commun.* 2 (2012) 75– 78.
- [46] N.Q. Chinh, R.Z. Valiev, X. Sauvage, G. Varga, K. Havancsák, M. Kawasaki, B.B. Straumal, T.G. Langdon, *Adv. Mater. Eng.* 16 (2014) 1000– 1009.
- [47] W.L. Chan, M.W. Fu, J. Lu, J.G. Liu, *Mater. Sci. Eng. A527* (2010) 6638– 6648.

- [48] E.O. Hall, Proc. Phys. Soc. London B64 (1951) 747– 752.
- [49] N.J. Petch, J. Iron Steel Inst. 174 (1953) 25– 28.
- [50] N. Hansen, Scripta Mater. 51 (2004) 801– 806.
- [51] J. Gil Sevillano, P. van Houtte, E. Aernoudt, Prog. Mater. Sci. 25 (1981) 69– 134.
- [52] G.I. Taylor, J. Inst. Metals 62 (1938) 307– 324.
- [53] J. Diehl, Z. Metallk. 47 (1956) 331– 343.
- [54] A. Messner, U. Engel, R. Kals, F. Vollersen, J. Mater. Process. Tech. 45 (1994) 371– 376.
- [55] W.L. Chan, M.W. Fu, J. Lu, Mater. Des. 32 (2011) 198– 206.
- [56] J.R. Greer, J.T.M.D. Hosson, Prog. Mater. Sci. 56 (2011) 654– 724.
- [57] C. Keller, E. Hug, A.M. Habraken, I. Duchêne, Int. J. Plasticity 64 (2015) 26– 39.
- [58] M.A. Meyers, E. Ashworth, Philos. Mag. 46 (1982) 737– 759.
- [59] L.F. Peng, X.M. Lai, H.J. Lee, J.H. Song, J. Ni, Mater. Sci. Eng. A526 (2009) 93– 99.
- [60] Y. Wang, P. Dong, Z. Xu, H. Yan, J. Wu, J. Wang, Mater. Des. 31 (2010) 1010– 1014.
- [61] E. Hug, C. Keller, Metall. Mater. Trans. A41 (2010) 2498– 2506.
- [62] T.G. Langdon, Metall. Trans. 3 (1972) 797– 801.
- [63] C. Xu, S. Schroeder, P.B. Berbon, T.G. Langdon, Acta Mater. 58 (2010) 1379– 1386.
- [64] R.Z. Valiev, T.G. Langdon, Metall. Mater. Trans. 42A (2011) 2943– 2951.
- [65] G. Sakai, K. Nakamura, Z. Horita, T.G. Langdon, Mater. Sci. Eng. A406 (2005) 268– 273.
- [66] R. Pippan, S. Scheriau, A. Hohenwarter, M. Hafok, Mater. Sci. Forum 584-586 (2008) 16– 21.
- [67] K. Edalati, Z. Horita, J. Mater. Sci. 45 (2010) 4578– 4582.

Figure and Table captions

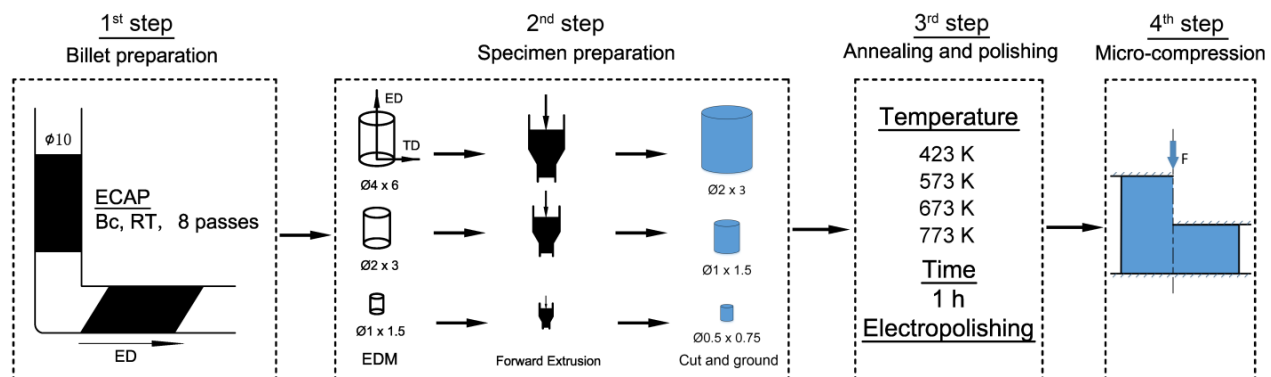


Fig. 1 Schematic illustration of the four stages of specimen preparation for micro-compression testing

(unit: mm)

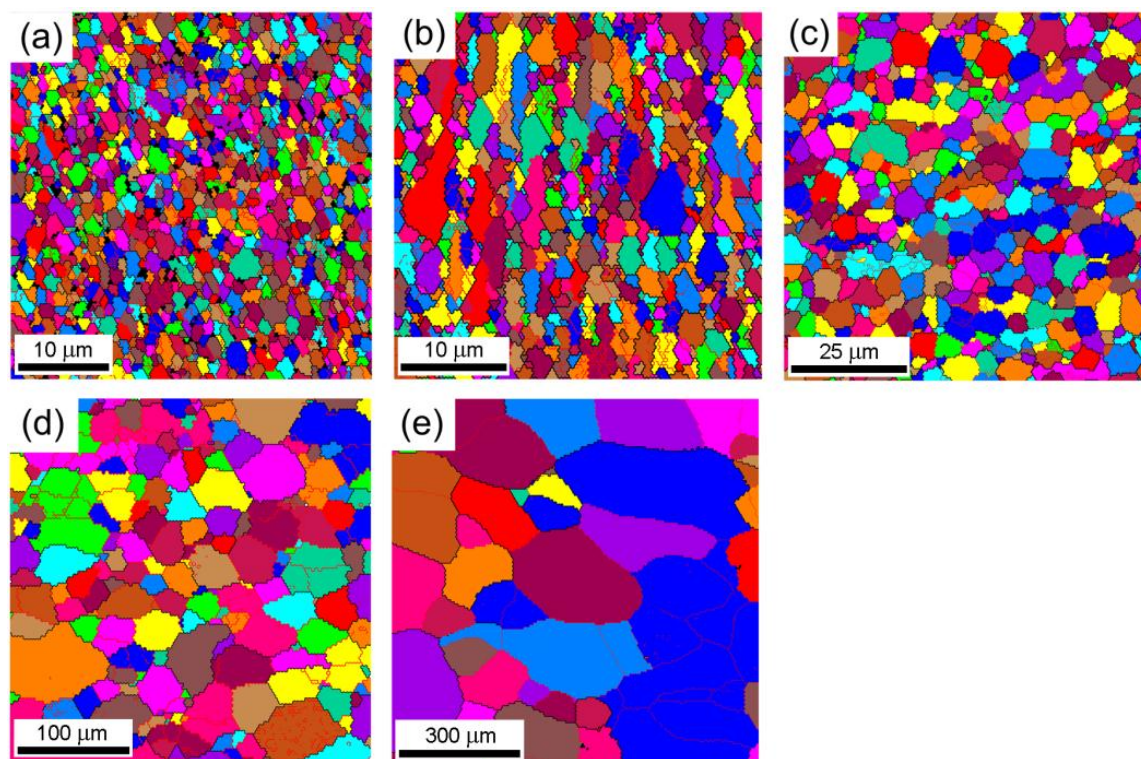


Fig. 2 OIM images for micro-compression specimens (a) without annealing and after annealing for 1 hour at (b) 423, (c) 573, (d) 673 and (e) 773 K.

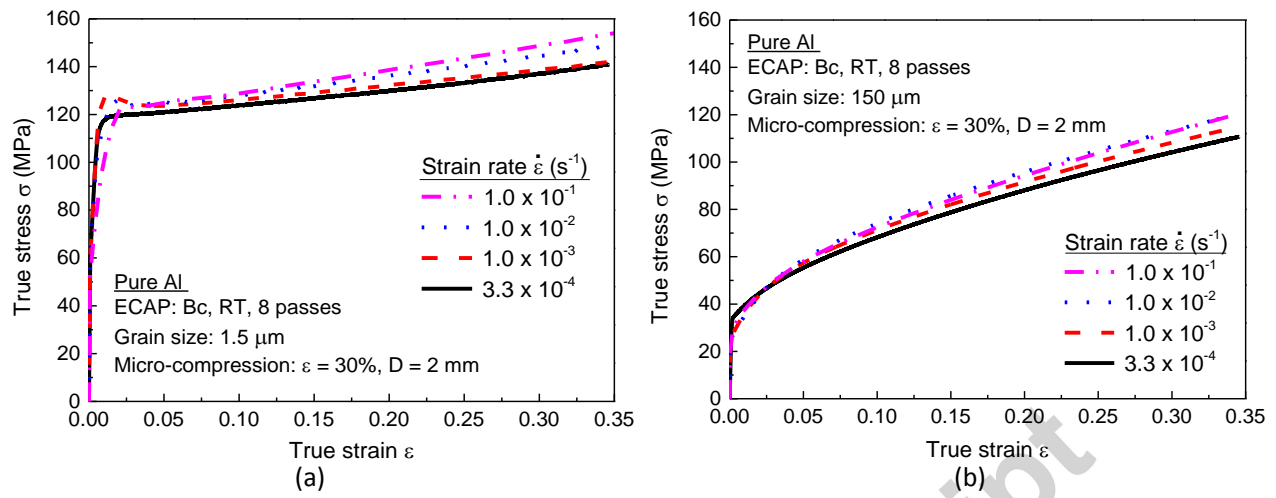


Fig. 3 Effect of strain rate on flow stress in micro-compression of pure Al with average grain sizes of (a) 1.5 and (b) 150 μm .

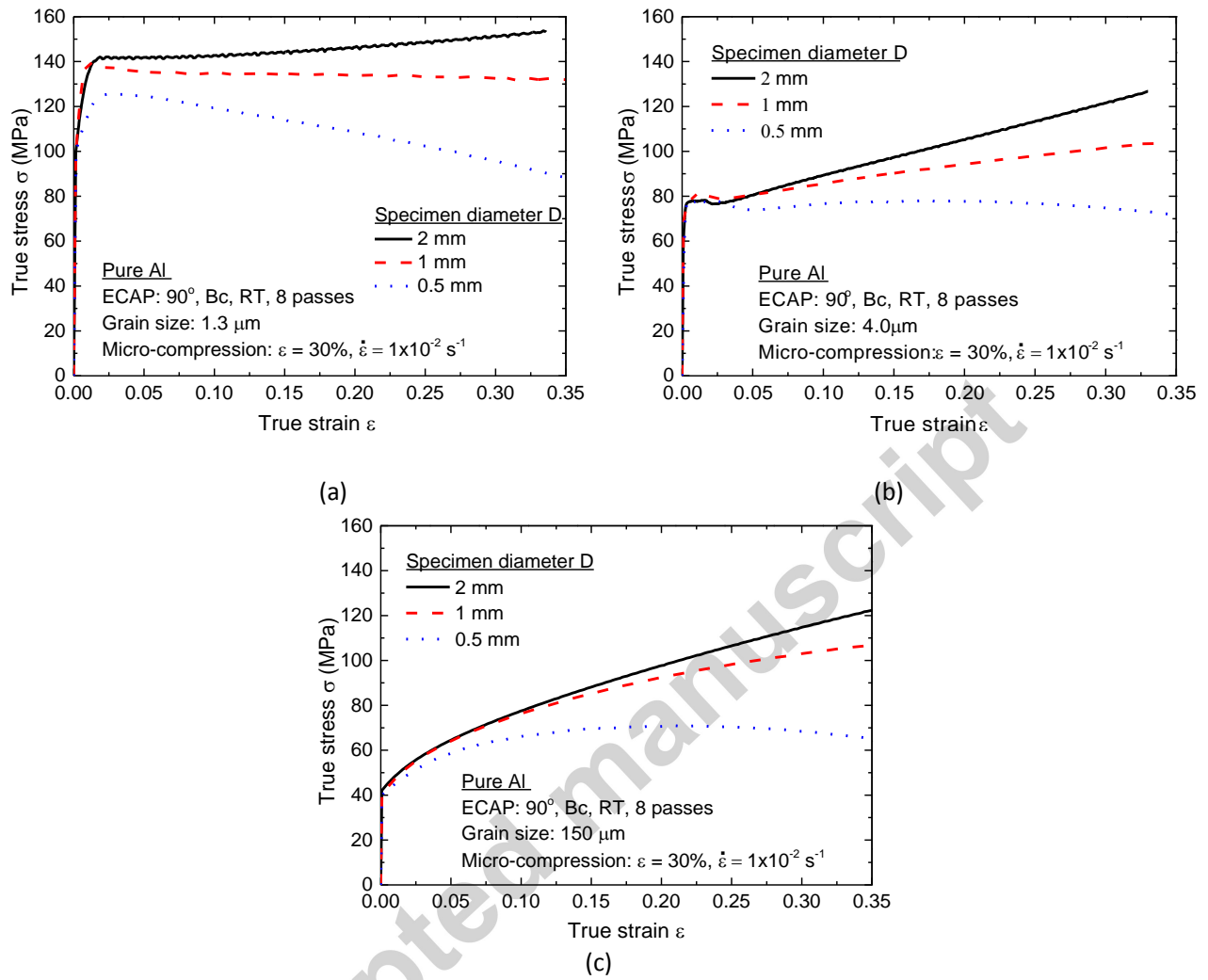


Fig. 4 True stress versus true strain for different specimen diameters for micro-compression samples having grain sizes of (a) 1.3, (b) 4 and (c) 150 μm .

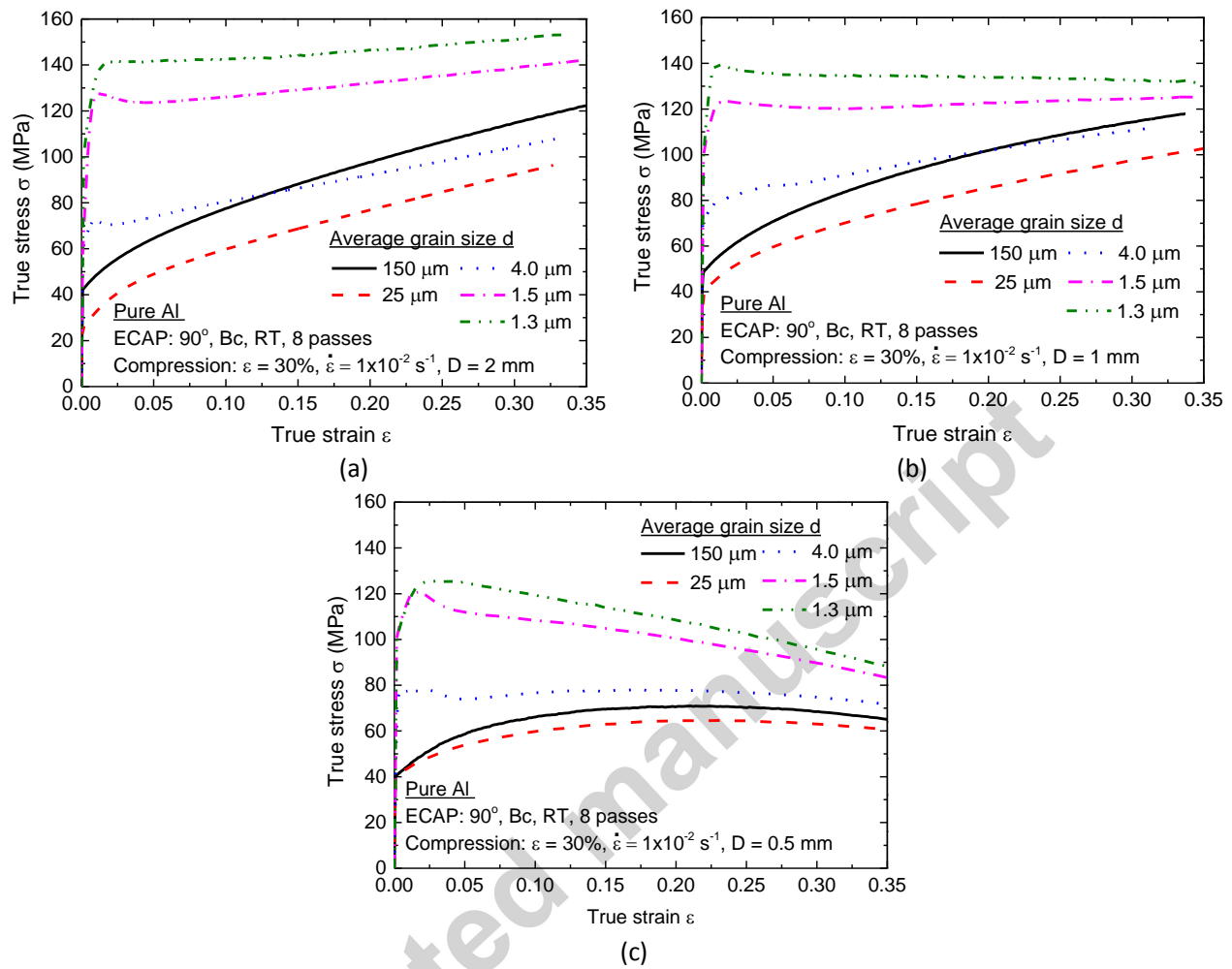


Fig. 5 True stress versus true strain in micro-compression testing with different grain size for specimen diameters of (a) 2, (b) 1 and (c) 0.5 mm.

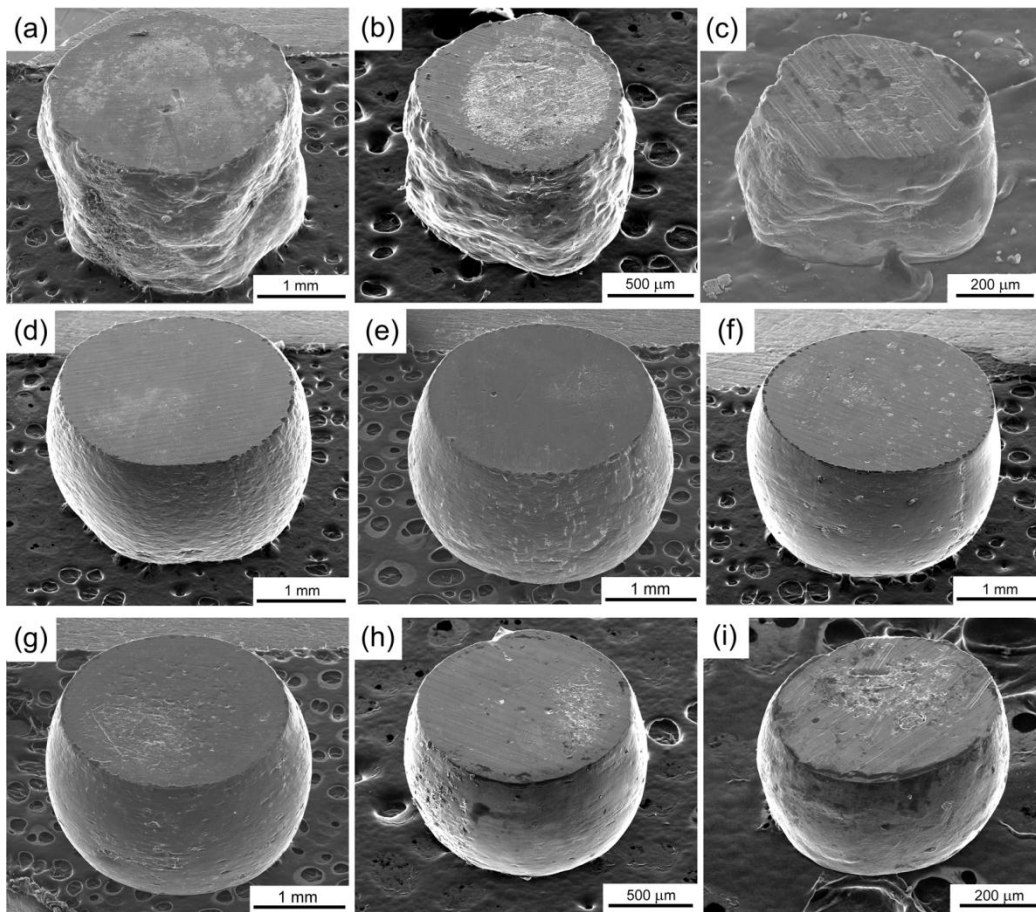


Fig. 6 SEM images of the compressed specimens having different specimen diameter, D , and grain size, d : (a) $D = 2$ mm, $d = 150$ μm ; (b) $D = 1$ mm, $d = 150$ μm ; (c) $D = 0.5$ mm, $d = 150$ μm ; (d) $D = 2$ mm, $d = 25$ μm ; (e) $D = 2$ mm, $d = 4$ μm (f) $D = 2$ mm, $d = 1.5$ μm ; (g) $D = 2$ mm, $d = 1.3$ μm ; (h) $D = 1$ mm, $d = 1.3$ μm ; (i) $D = 0.5$ mm, $d = 1.3$ μm .

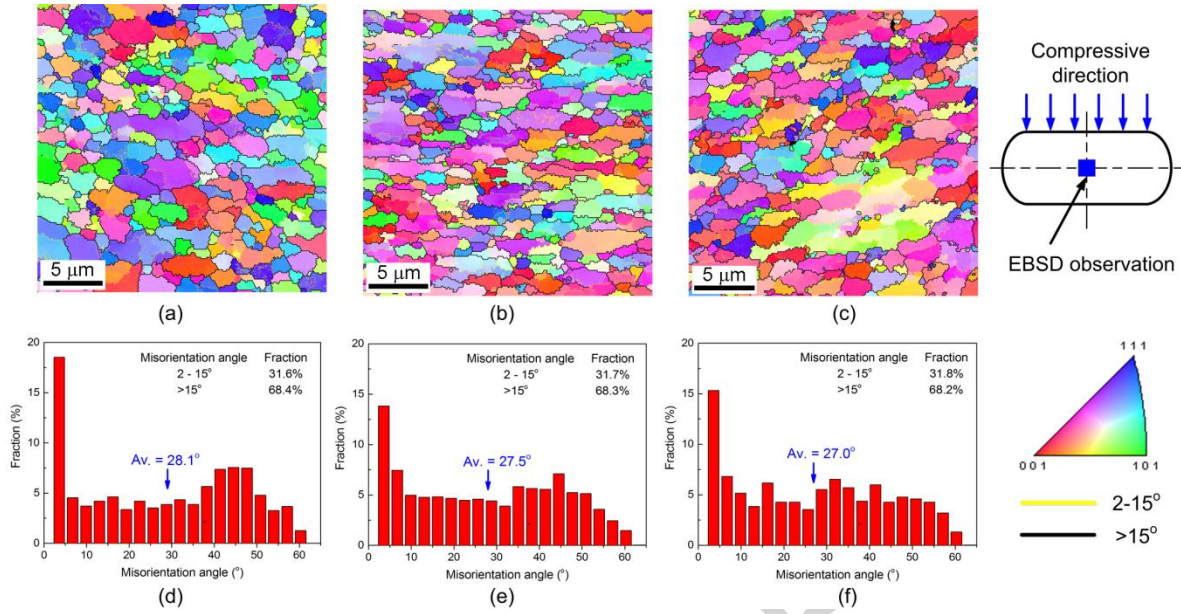


Fig. 7 Microstructures and misorientation angle distributions along the compressive direction at the centers of compressed samples having diameters of (a) 2, (b) 1 and (c) 0.5 mm using UFG pure Al with a grain size of 1.5 μm

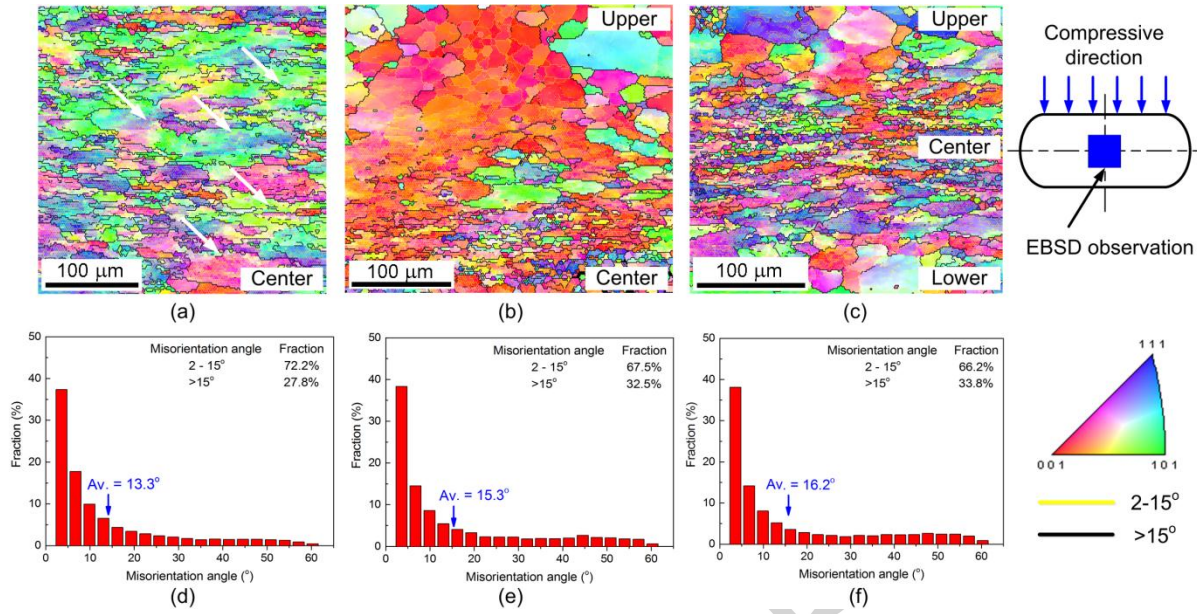


Fig. 8 Microstructure and misorientation angle distributions along the compressive direction at the centers of compressed samples having diameters of (a) 2, (b) 1 and (c) 0.5 mm using CG pure Al with a grain size of 25 μm.

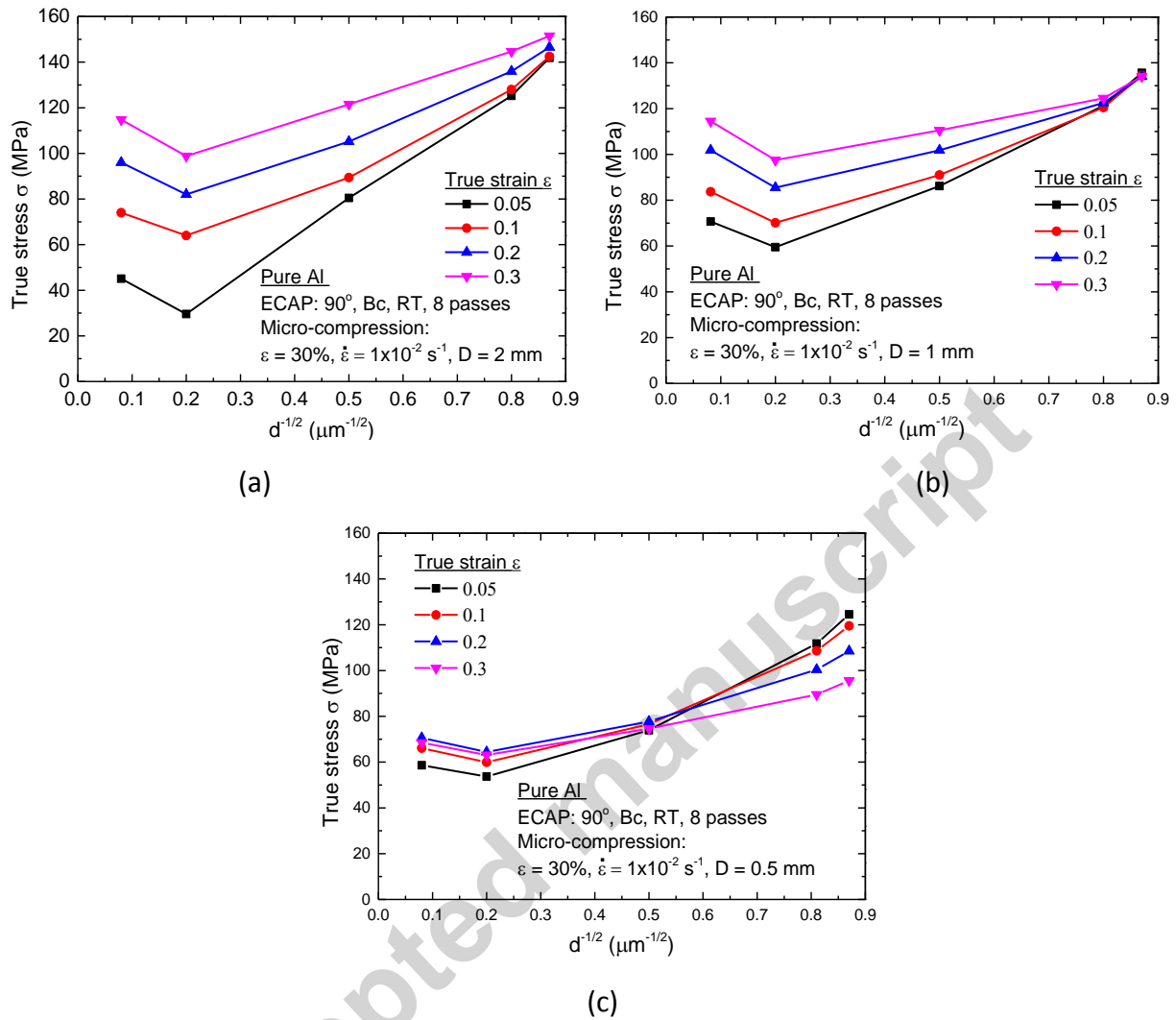


Fig. 9 The Hall-Petch relationship in micro-compression using different specimen sizes of (a) 2, (b) 1 and (c) 0.5 mm.

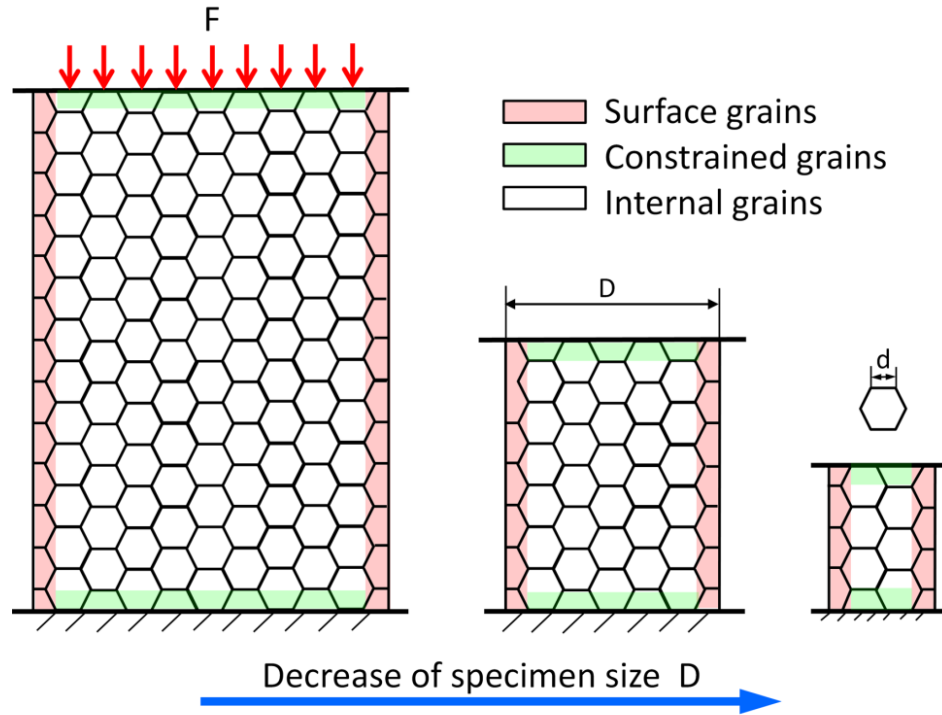


Fig. 10 A surface layer model showing the presence of surface grains, constrained grains and internal grains.

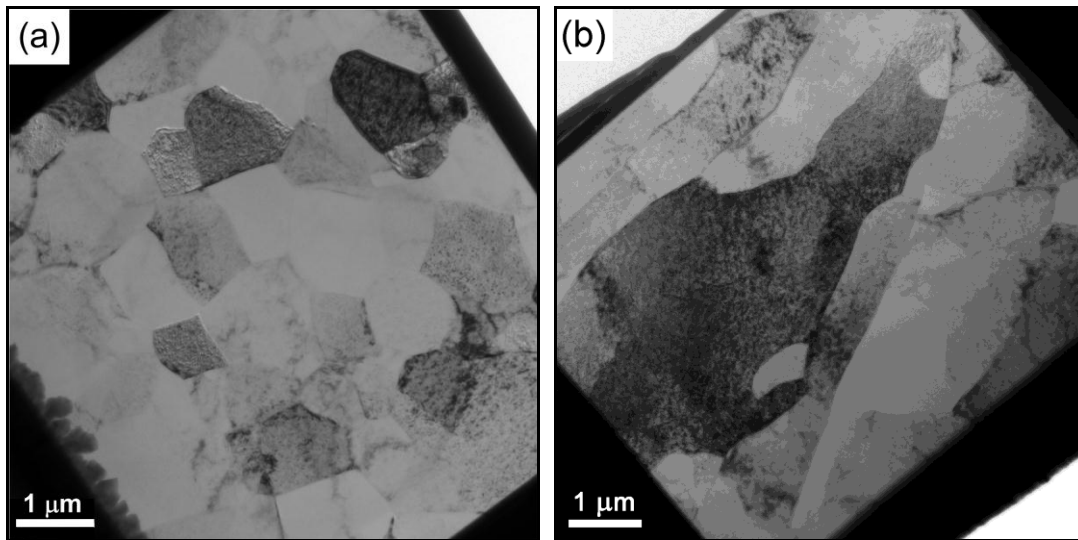


Fig. 11 TEM micrographs at the centers of samples after micro-compression of pure Al with average grain sizes of (a) 1.5 and (b) 25 μm .

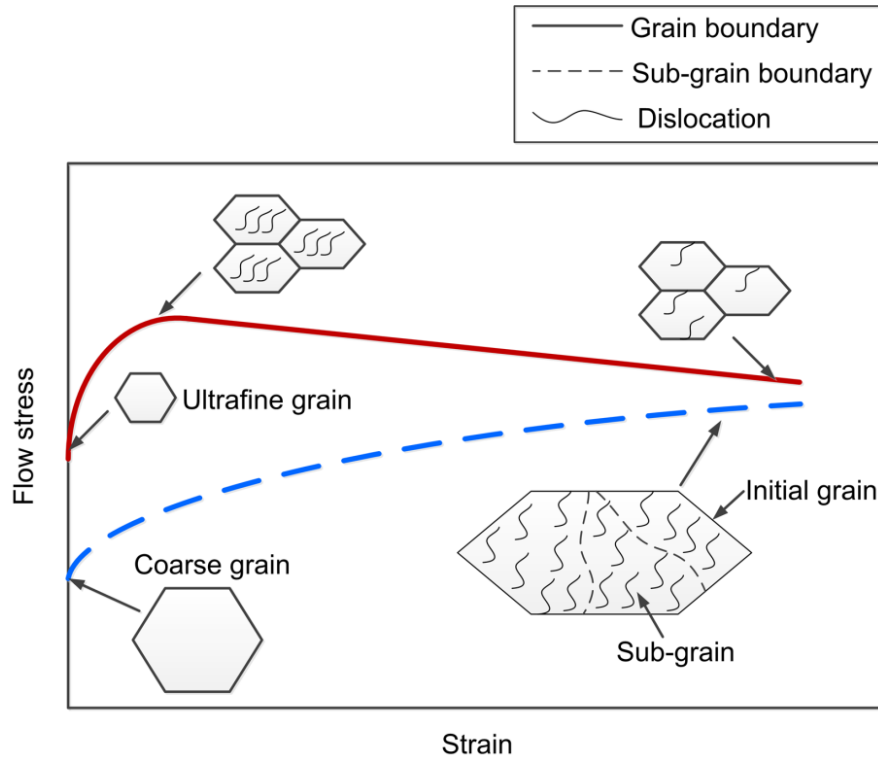


Fig. 12 Schematic illustration of the variations of flow stress with strain for coarse grains and ultrafine grains tested in micro-compression.

Table 1 Data for pure Al processed by ECAP without and with annealing treatments.

Annealing condition	Without annealing	423 K, 1h	573 K, 1h	673 K, 1h	773 K, 1h
Grain size (μm)	~1.3	~1.5	~4.0	~25	~150
Fraction of LAGBs (%)	29	33	32	52	68
Fraction of HAGBs (%)	71	67	68	48	32
Taylor factor	3.06	3.11	2.65	2.64	3.19